Astron. Astrophys. 360, 76–84 (2000)

ASTRONOMY AND ASTROPHYSICS

The dark and luminous matter coupling in the formation of spheroids: a SPH investigation

C. Lia[1], **G. Carraro**[2], **and P. Salucci**[1]

[1] SISSA/ISAS, Via Beirut 2, 34013 Trieste, Italy
[2] Department of Astronomy, Padova University, Vicolo dell'Osservatorio 5, 35122 Padova, Italy (liac,salucci@sissa.it; carraro@pd.astro.it)

Received 16 February 2000 / Accepted 30 May 2000

Abstract. Using N–body/hydrodynamical simulations which include prescriptions for star formation, feed-back and chemical evolution, we explore the interaction between baryons and dark matter (DM) at a galactic scale. The N–body simulations we performed using a Tree–SPH code that follows the evolution of individual DM halos inside which stars form from cooling gas, and evolve, delivering in the interstellar medium (ISM) mass, both metals and energy. We examine the formation and evolution of a giant and a dwarf elliptical galaxy of total masses $10^{12} M_{\odot}$ and $10^{9} M_{\odot}$, respectively. Starting from an initial density profile like the universal Navarro et al. (1996) profile in the inner region, baryons sink towards the center due to cooling energy losses. At the end of the collapse, the innermost part ($\simeq 1/20$ of the halo size) of the galaxy is baryon-dominated, whereas the outer regions are DM dominated. The star formation proceeds at a much faster speed in the giant galaxy where a spheroid of $8 \times 10^{10} M_{\odot}$ is formed in $2\ Gyr$, with respect to the dwarf galaxy where the spheroid of $2 \times 10^{7} M_{\odot}$ is formed in $4\ Gyr$. For the two objects the final distributions of stars are well fitted by a Hernquist profile with effective radii of $r_e = 30$ kpc and 2.8 kpc, respectively. The dark-to-luminous transition radius r_{IBD} occurs roughly at $1\, r_e$, as in real ellipticals. The DM halo density evolution is non-adiabatic and does not lead to a core radius.

Key words: methods: N-body simulations – galaxies: formation – galaxies: dwarf

1. Introduction

Galaxies of any morphological type and luminosity are known to be surrounded by DM halos, whose properties are remarkably universal (Salucci & Persic 1997 and references therein). The presence of DM halos has been detected through a variety of observational methods (Danziger 1997), from rotation curves in spirals (Giraud 2000, Swaters 1999, Persic et al. 1996) to M/L ratios in ellipticals (Bertola et al. 1993, Loewenstein & White III 1999 and references therein). To summarize, the properties of DM halos can be described as follows (Salucci & Persic 1997):

- dark and visible matter are well mixed already inside the luminous region of the galaxy;
- the transition radius R_{IBD} between the inner, baryon dominated region, and the outer, DM dominated region, moves inward progressively with decreasing luminosity;
- a halo core radius, comparable with the optical radius, is detected at all luminosities and for all morphologies;
- the luminous mass fraction varies with luminosity in a fashion common to all galaxy types: it is comparable with the cosmological baryon fraction at $L \simeq L_{\star}$, but it decreases by about a factor of 100 at $L \ll L_{\star}$;
- finally, for any Hubble type, the central halo density increases with decreasing luminosity.

Attempts to model the properties of DM halos in a cosmological context with N–body simulations trace back to Dubinski & Carlberg (1991) in the frame of cold dark matter (CDM) theory. The halos were found to be strongly triaxial and to exhibit a power law density profile varying from -1 in the center to -4 in the outskirts (Hernquist 1990 profile). Then, Navarro et al. (1996) (hereafter NFW), found that, independently from the adopted initial perturbation spectrum, the cosmological model and the halo mass, all DM halos possess the same *universal* density profile, fitted by the formula

$$\frac{\rho_r}{\rho_{crit}} = \frac{\delta_c}{(r/r_s)^a (1 + r/r_s)^{3-a}}, \qquad (1)$$

where $a = 1$, $\rho_{crit} = 3H_o^2/8\pi G$ is the critical density for closure, δ_c is a dimensionless characteristic density, and r_s is a scale radius, which defines where the profile shape has a slope of -2.[1]

This profile has a spike in the center of the halo, and differs in its asymptotic behavior from the Hernquist profile, decreasing as r^{-3} far from the halo center. Other simulations, with higher resolution and/or different initial conditions, confirmed the basic features of these findings, but disagreed with respect to some important aspects (Cole & Lacey 1996, Moore et al. 1997, van der Bosh, 1999). In fact, there are claims that the *universality* of the functional form (1) arises as a direct consequence of the hierarchical merging history of CDM halos (Syer & White (1997), or as a more generic feature of gravitational

Send offprint requests to: G. Carraro (carraro@pd.astro.it)

[1] * We take as Hubble's constant $H_o = 75\ Km/sec/Mpc$.

collapse (Huss et al. 1999). However, recently, the steepness of the central cusp has been found to vary significantly among different realizations, i.e. among halos (Jing & Suto 2000). It now seems likely that, CDM halos follow Eq. (1) with $a \simeq 1.5$ but with large variations of r_s with mass and also at a given halo mass.

On the other hand, a large discrepancy exists between CDM halo predictions and DM observations (Salucci & Persic 1997). Halos around galaxies show a density distribution which is inconsistent with Eq. (1). In particular, they have a density central core larger than the stellar scale-length and their density is:

$$\rho_h(r) \propto \frac{1}{(r+r_0)(r_0^2+r^2)}$$

with $r_0 \gg r_e$, r_e being the effective radius.

The disagreement between theory and observations on the mass distribution, and the existence of global scaling laws that couple the dark and the luminous matter (Persic et al. 1996) prompt the investigation of the past dynamical history of galaxies.

N-body/hydrodynamical simulations are an effective tool to obtain crucial information on the late stages of galaxy formation which is in some sense orthogonal to that we obtain with semi-analitycal methods or that we infer from observations. In fact, such simulations can account for the "physical" interaction between gas and dark matter. Moreover, many relevant physical processes occurring in the baryonic components, like thermal shocks, pressure forces and dissipation are explicitly taken into account.

The layout of the paper is as follow. In Sect. 2 we briefly describe the numerical tool, in Sect. 3 we discuss the initial conditions. In Sects. 4 and 5 we show the evolution of a giant and a dwarf elliptical, respectively. Finally, Sect. 6 summarizes the results.

2. The code

The simulations we present here have been performed by means of the Tree–SPH code developed by Carraro (et al. 1998), Buonomo et al. (2000) and Lia & Carraro (2000). The code, which is able to follow the evolution of a mix of CDM and Baryons (gas and stars), has been successfully checked against standard tests in Carraro et al. (1998), while a fine exploration of the parameters space is presented in Buonomo et al. (2000).

In detail, the gas component is "followed" by means of the smoothed particle hydrodynamics (SPH) technique (Lucy 1977; Gingold & Monaghan 1997; Hernquist & Katz 1989; Steinmetz & Müller 1993), while the gravitational forces are taken into account by means of the hierarchical tree algorithm of Barnes & Hut (1986). We adopt a tolerance parameter $\theta = 0.8$, a Plummer softening parameter and expand the tree nodes to quadrupole order.

In SPH each particle represents a fluid element whose position, velocity, energy, density etc. are followed in time and space. The properties of the fluid are locally estimated by an interpolation which involves the smoothing length h_i. Each particle possesses its own time and space variable smoothing length h_i, and evolves with its own time-step. This renders the code highly adaptive and flexible, and suited for numerical "experiments".

Radiative cooling is considered as a function of temperature and metallicity following Sutherland & Dopita (1993) and Hollenbach & McKee (1979) and the code takes into account the variations in metallicity among the fluid elements as a function of time and position.

Star formation (SF) and feed-back algorithms are described in Buonomo et al. (2000). Specifically SF, following partly Katz (1992), is set to occur when

$$t_{sound} > t_{ff}$$

and

$$t_{cooling} \ll t_{ff}$$

with the star formation rate of

$$SFR = \frac{d\rho_*}{dt} = -\frac{d\rho_g}{dt} = \frac{c_*\rho_g}{t_g}$$

where c_* is the dimensionless efficiency of star formation, and t_g is the characteristic time for the gas to flow, usually set to the maximum between the cooling time and the free-fall time. For the simulations discussed here, we keep $c_* = 1.0$. When formed, stars are distributed in mass according to the Miller & Scalo (1979) initial mass function (IMF).

The effects of energy (and mass) feed-back from supernovae and stellar winds are also taken into account (Chiosi & Maeder 1986, Thornton et al. 1998). In this experiments we deposit all the energy released by SNæ ($10^{49}\, erg$) and stellar wind in the thermal budget of the bubble, following the kind of arguments discussed in Buonomo et al. (2000).

Finally, the chemical enrichment of the interstellar gas caused by the the stellar wind and ejecta is followed by means of the closed-box model applied to each gas-particle as in Carraro et al. (1998). Metals are then SPH-diluted over the surrounding gas particles.

3. Initial conditions

The code follows the dynamical formation of galaxies since the moment in which the protohalo detaches itself from the Hubble flow with its cosmological share of baryonic material. Thus, we set *ad hoc* initial configuration for a protogalaxy and let the system evolve within the SPH scheme described above. Moreover, we assume that the star formation starts after the dark halo is virialized.

This approach is justified on the grounds that in this paper, we aimed to 1) test a simple but reasonable initial conditions set-up and 2) focus on processes which occur mainly at scales much smaller than the halo virial radius.

The working scenario is that, after a violent relaxation process which follows the separation from the Hubble expansion, the DM halo acquires a particular density distribution, and then accretes baryonic material which heats up to the halo virial temperature. Gas then radiatively cools and collapses, and through

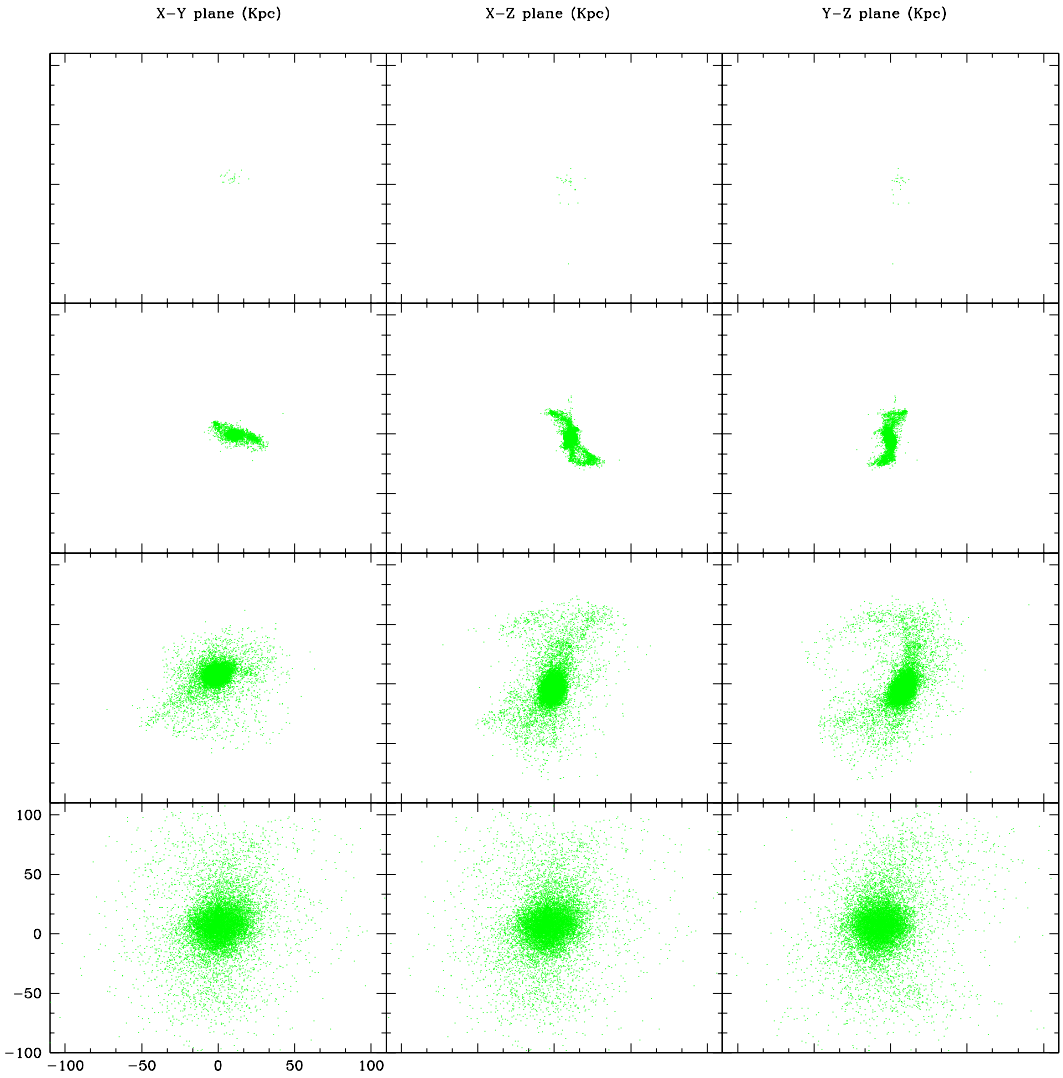

Fig. 1. The formation of a giant elliptical. From the top to the bottom, snapshots refer to 1, 2, 3 and 9 Gyrs.

fragmentation, turns into the stars we see today in disks and spheroidal systems.

This scenario is not incompatible with the merging one, withstanding that the baryonic collapse takes place after the last merging episode.

4. Initial configuration

We set up a protogalaxy as an isolated virialized DM halo with baryonic material inside it. We assume spherical, isotropic and non-rotating halos of density profiles:

$$\rho(r) \propto \frac{1}{r}. \tag{2}$$

Notethat Eq. (2) matches the profile of CDM halos in the innermost regions, especially in low Ω Universe for which $r_s \sim$ 10–30 kpc. Different profiles, more in line with observations or theoretical claims, will be considered in forthcoming papers.

Gravitational interaction is modeled by adopting a Plummer softening constant over the simulation and is equal for both DM and gas. By plotting the inter-particles separation as a function of the galactocentric distance, we derive the softening parameter ϵ as the mean inter-particles separation at the center of the sphere, taking at least one hundred particles inside the softening radius.

DM particles (10,000 in number) are distributed inside a sphere according to an *acceptance–rejection* procedure for generating random deviations with a known distribution function (Press et al. 1989).

Along with positions, we also assign the isotropic dispersion velocity $\sigma(r)$ according to:

$$\sigma^2(r) \propto (rln(\frac{1}{r})). \tag{3}$$

which is the solution of the Jeans equation for spherical isotropic collisionless system with the density profile of Eq. (2).

Fixing the total mass of the system M_{200}, we assume that a radius

$$R_{200} \equiv (\frac{3}{4\pi})^{1/3}(\frac{M_{200}}{200\rho_c})^{1/3} \gg r_e$$

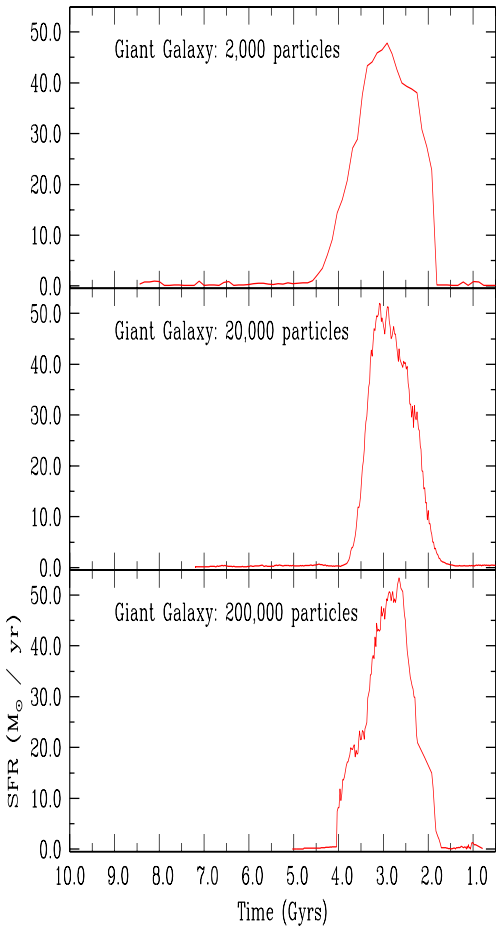

Fig. 2. SF for the giant elliptical as a function of time. From the top to the bottom the same model is shown at increasing number of particles, i.e at increasing resolution.

Table 1. Properties of the virialised primordial DM halos.

$Mass$	T_{vir}	R_{200}
$10^{10}M_{\odot}$	$10^5\ ^oK$	kpc
100	3.8	256
0.1	1.2	30

truncates the dark halo, where ρ_c is the critical density to close the Universe.

The systems are then allowed to evolve until virial equilibrium is reached. 10,000 baryonic particles are then homogeneously distributed inside the DM halo with zero velocity field and low metal content ($Z = 10^{-4}$). The initial gas temperature is $10^4\ ^o$K.

5. A giant elliptical galaxy

In the first simulation we set a giant elliptical of gaseous mass of $10^{11}M_{\odot}$ to form through the collapse of a spherical DM halo of $10^{12}M_{\odot}$. Each gas particle has an initial mass of $10^7M_{\odot}$.

Looking at Figs. 1 and 2, baryons slowly infall towards the center of the potential well, gas condenses, cools and then finally, stars begin to form at a rate of $50M_{\odot}yr^{-1}$. The strong episode of star formation lasts for about 2 Gyr and it is marked by a large rate of production of SNæ of type II. These, however, are not able to expel from the galaxy a relevant fraction of the gas, given its strong gravitational field. At the end of this period, it has been processed into stars 80% of the original material. The remaining 20% is left partly in the outermost regions of the dark halo, partly out of the virial radius.

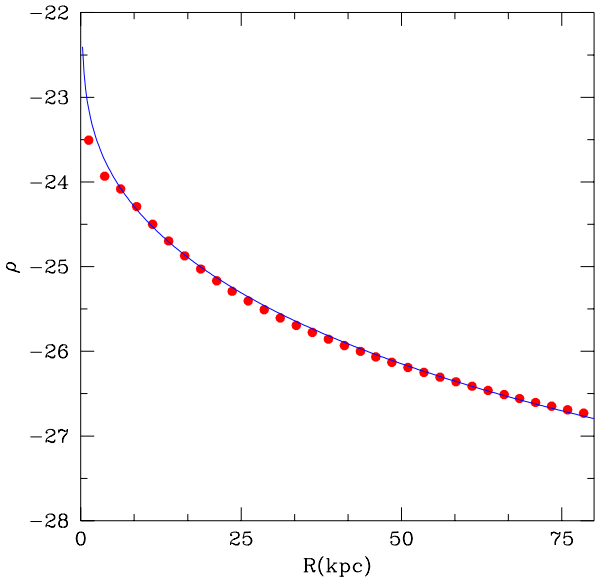

Fig. 3. Final stellar density profile of the giant galaxy. A Hernquist profile for $r_e = 30$ kpc is superimposed.

The collapse of baryons in the DM potential well can be realized by noting that, at $t = 0$, in the innermost 10 kpc of the protogalaxy, the DM halo is 10 times denser than the gaseous component but at the end of the formation of the spheroid, the stellar component reaches a "central" density 30 times that of the dark component.

Not surprisingly, the final distribution of stars does not follow that of the DM. In fact, as the infall proceeds, the DM remains C^{∞} scale-free, while the baryons develop a C^1 scale r_e of about one tenth of the virial radius. More precisely, the dissipative zero-angular momentum infall of the (out-to-250 kpc) scale-free baryonic material produces a half-mass scale-length of ~ 30 kpc. The final stellar distribution closely follows a Hernquist profile (see Fig. 3) with effective radius r_e slightly larger than that of ellipticals of the same baryonic mass. However, the simulated value of r_e depends on the assumed DM density and on the prescriptions of star formation. Actually, one could use the observed r_e vs stellar mass relationship to fine tune the semi-analytical parts of the code (Buonomo et al. 2000).

During the galaxy assembly a coupling between the baryons and the DM is created. The initial halo distribution $\rho(r,0) = M_{200}/(2\pi R_{200}^2)1/r$ first is slightly contracted by the baryonic infall and then expanded by a (limited) supernovae-driven outflow. As a result, the final DM distribution is not too different from the primordial one. On the other hand, the DM potential

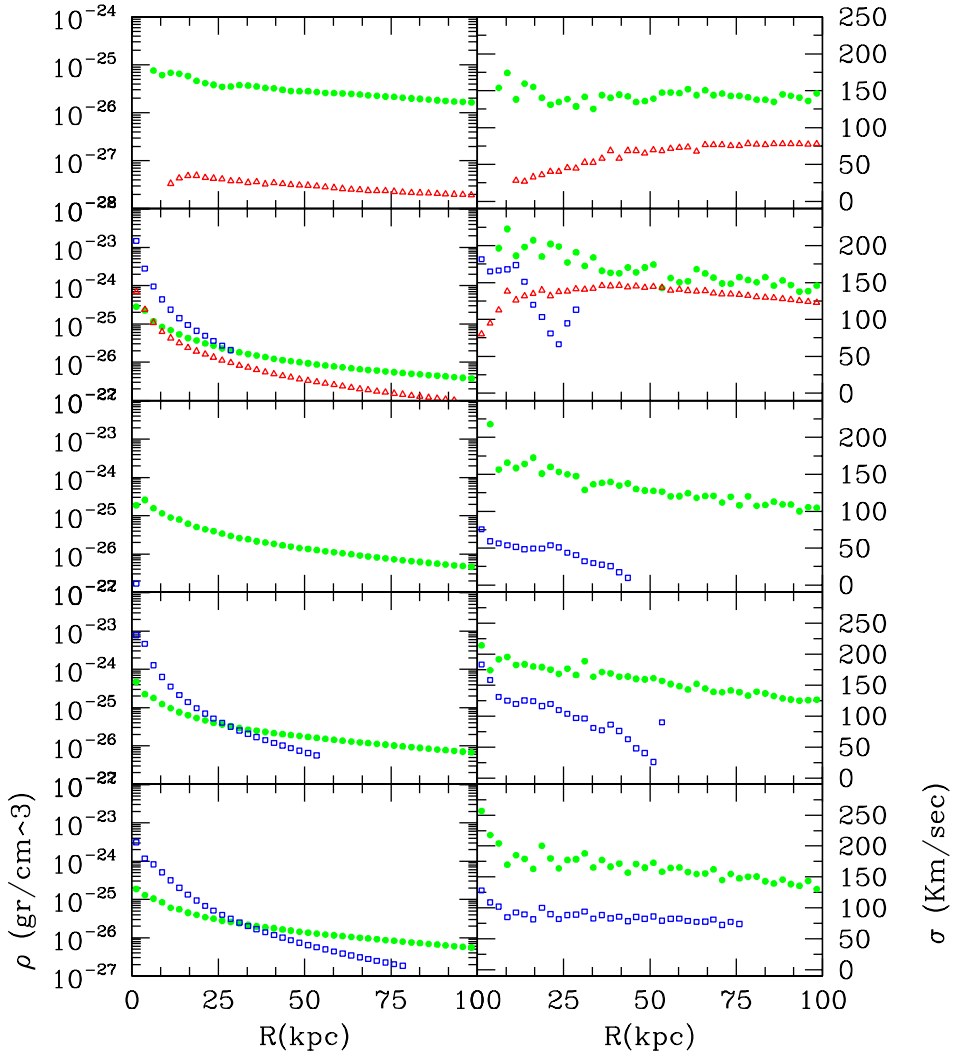

Fig. 4. Time evolution of the density and dispersion profiles. Solid circles stand for DM, open triangles for gas and open squares for stars. From the top to the bottom profiles refer to 1, 3, 3.5, 4.5 and 9 Gyr.

controls the star formation rate and efficiency, including the fate of stellar ejecta.

Even in the present simplified scenario, the time-evolution of the mass distribution is not that of an adiabatic process (Blumenthal et al. 1986). In fact, (see Fig. 5) the adiabatic invariant $rM(r)$ varies with time. In the innermost parts $r < 50$ kpc, it increases with time while, for larger radii, $r < 100$ kpc, it decreases as the collapse proceeds. The baryonic infall develops shell crossings as an effect of the strong radial dependence of the the energy (un)balance among cooling, heating and release of gravitational energy.

6. A dwarf elliptical galaxy

The second simulation concerns a proto-elliptical of gaseous mass of $10^8 M_\odot$ forming through the monolithic collapse of a spherical virialized DM halo of $M_{200} = 10^9 M_\odot$. In this case a gas particle has an initial mass of of $10^4 M_\odot$.

Despite the fact that the virial radius is now much smaller ($R_{200} = 35$ kpc), the gas is not more rapid in condensating, cooling and forming stars. Note that both the free-fall time and the cooling time are smaller.

The time evolution of the SFR in this case cannot be described as a a single burst, but rather as a series of several episodes, each one of about 0.5–$1 M_\odot yr^{-1}$, lasting for over 4 Gyr (see Figs. 6 and 7), a result which is in close agreement with observations of dwarf galaxies in the local group (Mateo 1998).

At the end of this period only 20% of the original materia it has been processed into long-living starsl. The remaining 80% has been thrown out from the galaxy or left, unprocessed, behind, in the outermost regions of the DM halo.

In the central regions, the baryonic density increases as the collapse proceeds to reach "at the center" 30 times the density of the dark component. The stellar scale-length is $r_e \sim 2.8$ kpc, which is not too different from that of ellipticals of the same baryonic mass (see Fig. 8). Also in this case, there is a clear coupling between baryons and DM during the galaxy assembly.

However, in this case, due to the weaker gravitational field, most of the gas gets expelled from the galaxy. The halo density evolves during the baryonic infall, in a non-adiabatic way, as

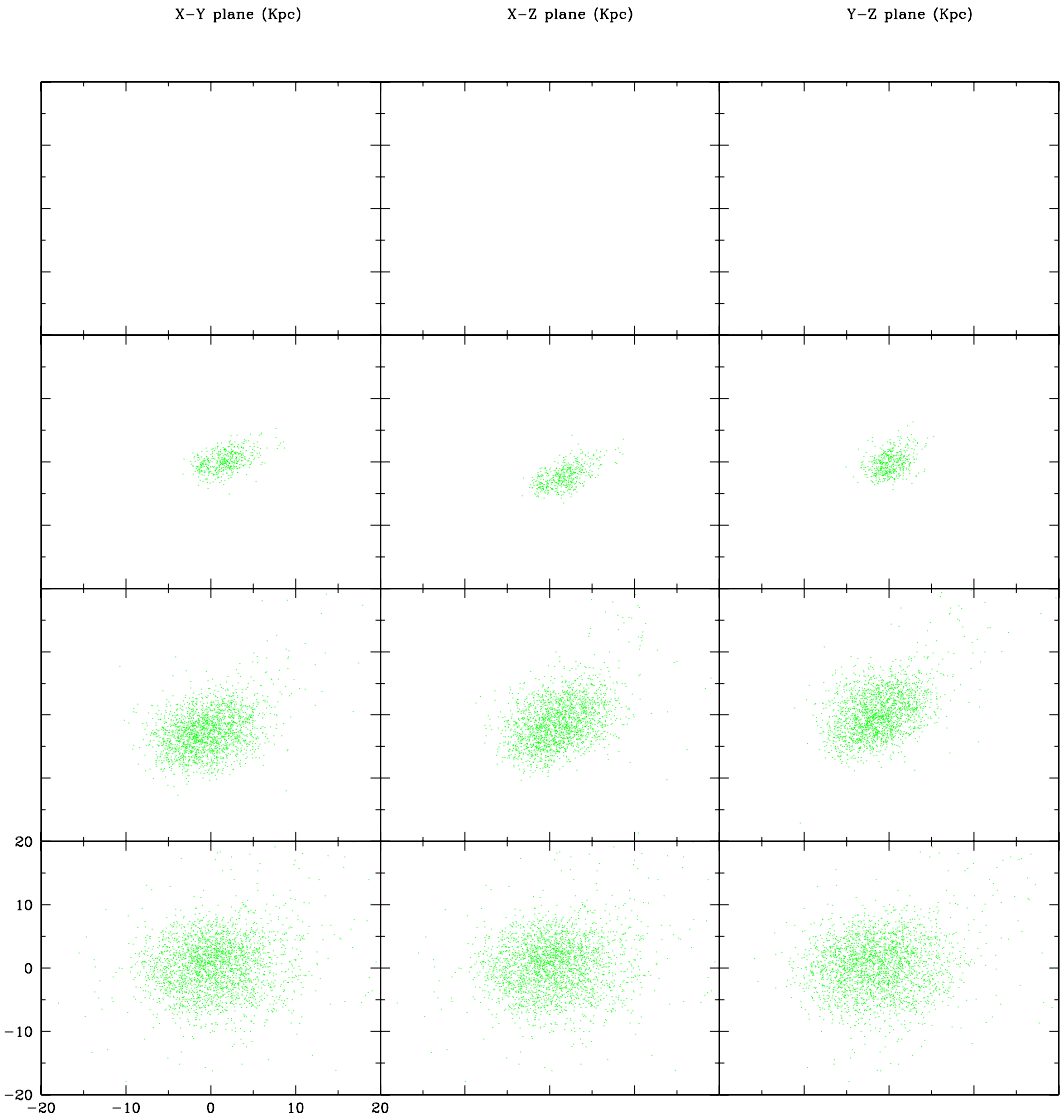

Fig. 5. The formation of a dwarf elliptical. From the top to the bottom, snapshots refer to 1, 2, 3 and 9 Gyrs.

shown in Fig. 9. The final DM distribution is not too different from the primordial one (see Fig. 10).

7. Discussion and conclusions

In this paper we have investigated the coupling between DM and baryons during an assumed monolithic formation of two galaxies: a giant and a dwarf spheroidal galaxy.

Starting from a homogeneous distribution, baryons sink toward the center of the virialized DM halo due to cooling instability. The smallest object has about 10 independent episodes of star formation $0.3\ Gyr$ long, while the largest has basically one single burst which is 10 times longer. This difference nicely matches the available observations. Giant elliptical galaxies are indeed old objects dominated by a single burst of star formation (Bender et al. 1992), whereas dwarf ellipticals basically exhibit an irregular and intermittent SF history (Mateo 1998).

A crucial and sensitive aspect of our simulations is that both the giant and the dwarf object have been modeled with the same number of particles, which implies an increase by a factor 10^3 in the mass resolution passing from the giant to the dwarf.

To check whether the results for the SF histories depend on the mass resolution of our simulations, the giant galaxy has been re-simulated using 2,000, 20,000 and 200,000 particles, whilst the dwarf galaxy has been re-simulated using 2,000 and 20,000 particles.

This way the mass resolution goes from 10^8 to $10^6 M_\odot$ for the giant galaxy, and from 10^5 to $10^4 M_\odot$ for the dwarf galaxy. The results are summarized in Fig. 2 and Fig. 7, where we compare the SF histories of the two galaxy models at increasing mass resolution.

In both cases we show a reasonable convergence of the results.

As for the giant galaxy (see Fig. 2), we show that the SF history is dominated by a single ancient burst of SF, whose trend

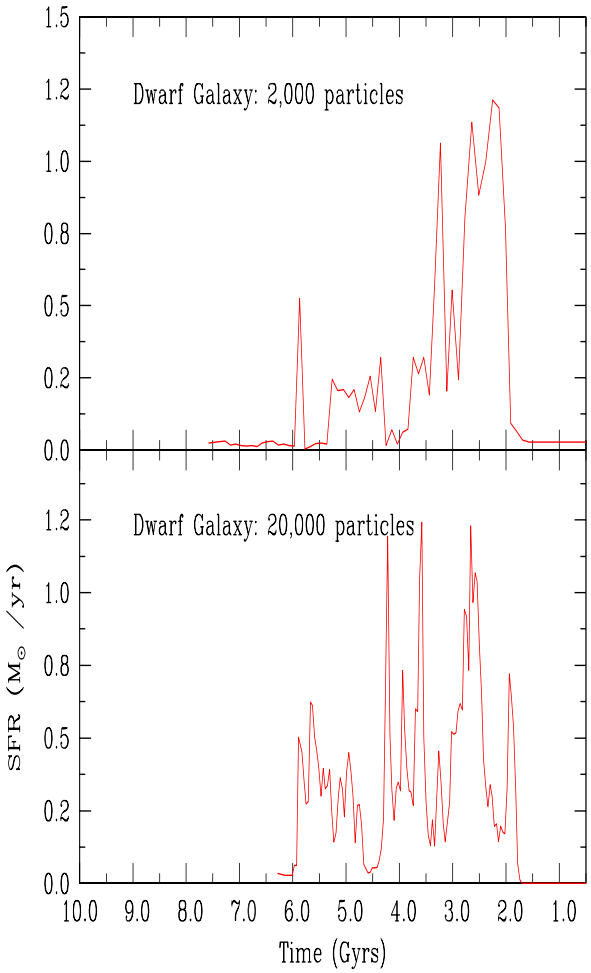

Fig. 6. SF history for the dwarf elliptical as a function of time. The two panels show the same model at increasing particle number.

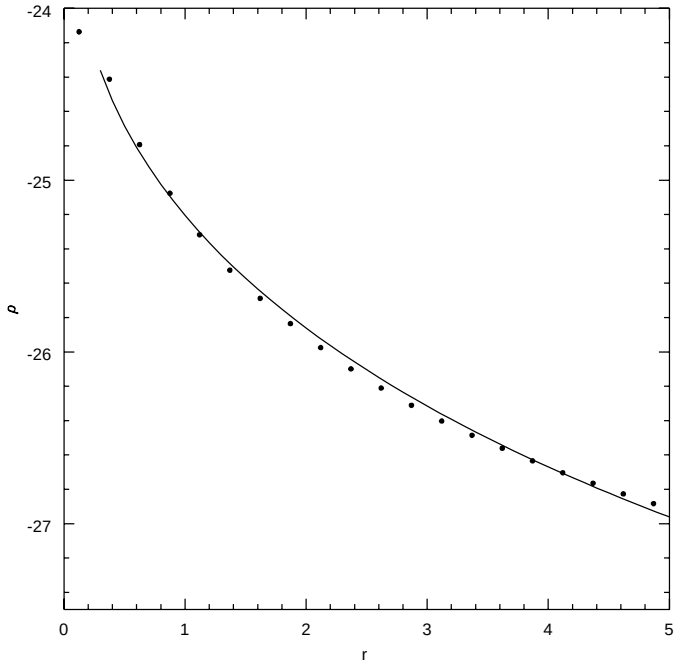

Fig. 7. Baryons final density profile. Superimposed is a Hernquist profile for $r_e = 2.8$ kpc.

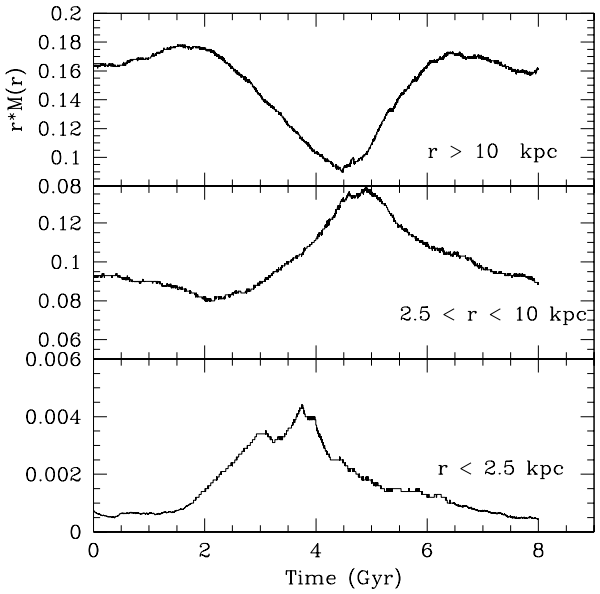

Fig. 8. Adiabatic invariant evolution for the dwarf galaxy in three different galaxy regions. $r \times M(r)$ is in code units.

does not change too much passing from 2,000 to 200,000 particles. Nevertheless, a more careful analysis shows that a difference emerges passing from 2,000 to 20,000 particles, whereas passing from 20,000 to 200,000 particles does not significantly change the global result.

Although the SF peak is almost the same in all the simulations, the low resolution run produces a burst larger than the other two cases. Correspondingly, the amount of gas consumed (and hence the final mass in stars) passes from 90% in the low resolution run to about 80% in the medium and high resolution run. This means that at increasing number of particles, the results asymptotically converges.

These conclusions confirm previous analyses on the performances of the SPH method (Steinmetz & Müller 1993, Thacker et al. 1998). By comparing different SPH implementations they find that the minimum number of particles required to calculate local physical variables in dynamically evolving systems is about 10,000, and that the SPH method can give reasonable results also by using a small number of particles.

On the other hand, changing the resolution by a factor of 10 does not alter the SF history of the dwarf galaxy (see Fig. 7), which exhibits several episodes of SF, although the number and position of the peaks does not coincide exactly.

The basic results of this paper can be summarized as follows:

- the stars which are formed show a final distribution which is greatly different from the DM distribution and can be represented by a Hernquist profile with a length-scale r_e;
- a particular aspect of the mass distribution is that the regions inside r_e are baryon dominated, while the DM is the main mass component at outer radii, as observed in real ellipticals;

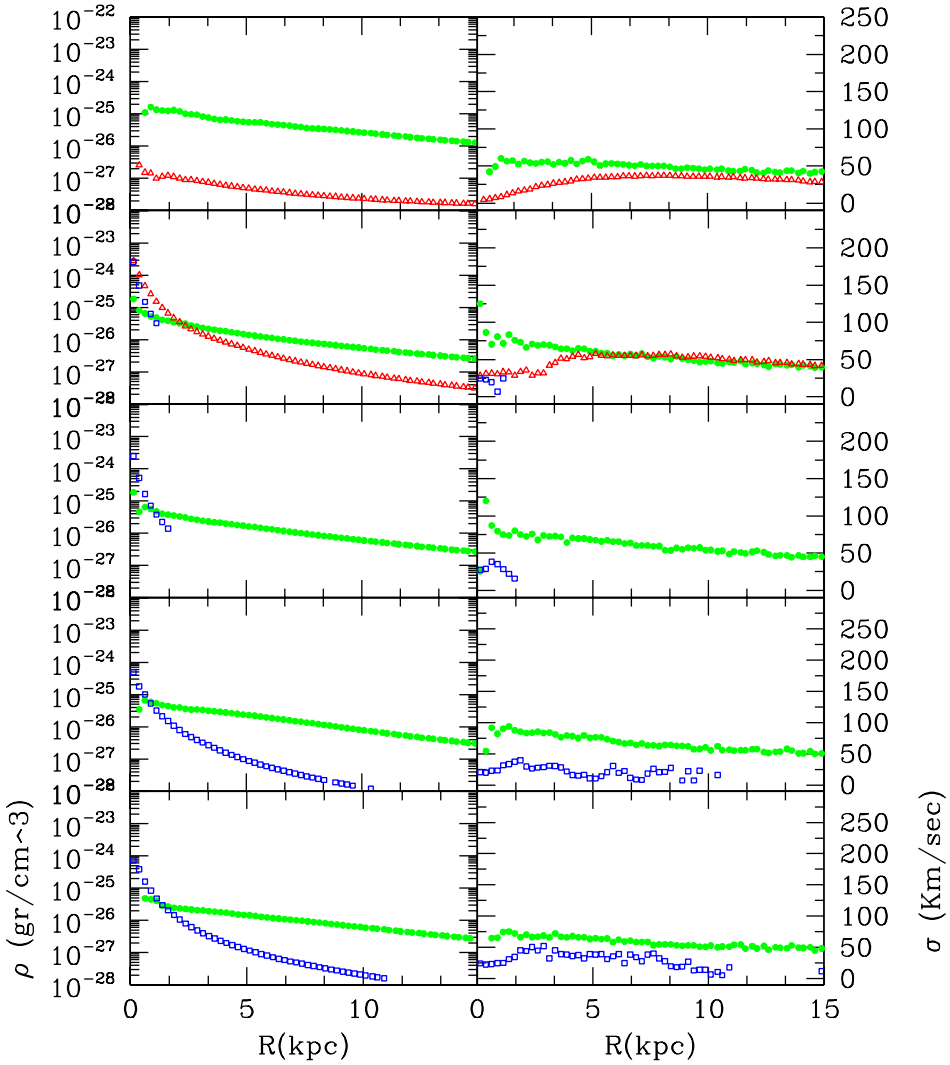

Fig. 9. Evolution of density and dispersion profiles for the Dwarf Elliptical Galaxy. Solid circles stand for DM, open triangles for gas and open squares for stars. From the top to the bottom profiles refer to 1.5, 2, 3.5, 5 and 9 Gyr.

- finally it is worth noting that, in both objects, the final DM velocity dispersion is about 1–2 times the stars velocity dispersion, in agreement with Loewenstein & White III (1999) findings.

In forthcoming papers we are going to analyze simulations which adopt different initial conditions for DM, in order to test the effect of the DM initial properties (density profile, velocity dispersion and so forth) on the final baryon distribution.

Acknowledgements. The authors acknowledge very useful discussions with Dr. E. Pignatelli and Prof. L. Danese. Moreover we thank an anonymous referee for his detailed comments on the first version of this paper. We acknowledge financial support from Italian Ministery of Research, University, Science and Technology (MURST).

References

Barnes J. E., Hut P., 1986, Nat 324, 446
Bender R., Burstein D., Faber S.M., 1992, ApJ 399, 462
Bertola F., Pizzella A., Persic M., Salucci P., 1993, ApJ 416, L45
Blumenthal G.R., Faber S.M., Flores R., Primack J.R. 1986, ApJ 301, 27
Buonomo F., Carraro G., Chiosi C., Lia C., 2000, MNRAS 312, 371
Carraro G., Lia C., Chiosi C., 1998, MNRAS 298, 1021
Chiosi C., Maeder A., 1986, ARA&A 24, 329
Cole S., Lacey C., 1997, MNRAS 281, 716
Danziger I.J., 1997, In: Persic M., Salucci P. (eds.) Dark and Visible Matter in Galaxies. ASP Vol. 117, p. 28
Dubinski J., Carlberg R., 1991, ApJ 378, 496
Gingold R.A., Monaghan J.J., 1977, MNRAS 181, 375
Giraud E., 2000, ApJ 531, 701
Hernquist L., 1990, ApJ 356, 359
Hernquist L., Katz N., 1999, ApJS 70, 419
Hollenback D., McKee C.F., 1979, ApJS 41, 555
Huss H., Jain B., Steinmetz M., 1999, ApJ 517, 64
Jing Y.P., Suto Y., 2000, ApJ 529, L69
Katz N., 1992, ApJ 391, 502
Lia C., Carraro G., 2000, MNRAS 314, 145
Loewenstein M., White III R.E, 1999, ApJ 518, 50
Lucy, L., 1977, AJ 82, 1013
Mateo M., 1998, ARA&A 36, 435
Miller G.E., Scalo J.M., 1979, ApJS 41, 513
Moore B., Governato F., Quinn T., Stadel J., Lake G., 1998, ApJ 462, 563
Navarro J.F., Frenk C.S., White S.D.M., 1996, ApJ 462, 563

Persic M., Salucci P., Stel F., 1996, MNRAS 281, 27
Press W.H., Flannery B.P., Teukolsky S.A., Vetterling W.T., 1989, Numerical Recipes. Cambridge University Press, Cambridge
Salucci P., Persic M., 1997, In: Persic M., Salucci P. (eds.) Dark and Visible Matter in Galaxies. ASP Vol. 117, p. 1
Steinmetz M., Müller E., 1993, A&A 268, 391
Sutherland R.S., Dopita M.A., 1993, ApJS 88, 253
Syer D., White S.D.M., 1998, MNRAS 293, 337
Swaters R., 1999, Ph.D. Thesis, Groningen University
Thacker R.J., Tittley E.R., Pearce F.R., Couchman H.M.P., Thomas P.A., 1998, astro-ph/9809221
Thornton K., Gaudlitz M., Janka H.-Th., Steinmetz M., 1998, ApJ 500, 95
van den Bosch, Robertson J.J., de Block W.J.G., 2000, astro-ph/9911372
Weil M.L., Eke V.R., Efstathiou G., 1998, MNRAS 300, 773